

Research



Cite this article: Li T-t, Bao N, Geng A-f, Yu H, Yang Y, Dong X-t. 2018 Study on room temperature gas-sensing performance of CuO film-decorated ordered porous ZnO composite by In₂O₃ sensitization. *R. Soc. open sci.* 5: 171788.

<http://dx.doi.org/10.1098/rsos.171788>

Received: 7 November 2017

Accepted: 8 January 2018

Subject Category:

Chemistry

Subject Areas:

materials science/nanotechnology

Keywords:

ordered mesoporous ZnO, electroplating after chemical plating method, CuO film, In₂O₃, NO_x, gas sensor

Authors for correspondence:

Ai-fang Geng

e-mail: gengaf0687@sina.com

Hui Yu

e-mail: yh2001101@163.com

This article has been edited by the Royal Society of Chemistry, including the commissioning, peer review process and editorial aspects up to the point of acceptance.

Electronic supplementary material is available online at <https://dx.doi.org/10.6084/m9.figshare.c.3986814>.



Study on room temperature gas-sensing performance of CuO film-decorated ordered porous ZnO composite by In₂O₃ sensitization

Tian-tian Li, Na Bao, Ai-fang Geng, Hui Yu, Ying Yang and Xiang-ting Dong

School of Chemistry and Environmental Engineering, Changchun University of Science and Technology, Changchun 130022, People's Republic of China

HY, 0000-0002-5413-3306

For the first time, ordered mesoporous ZnO nanoparticles have been synthesized by a template method. The electroplating after chemical plating method was creatively used to form copper film on the surface of the prepared ZnO, and then a CuO film-decorated ordered porous ZnO composite (CuO/ZnO) was obtained by a high-temperature oxidation method. In₂O₃ was loaded into the prepared CuO film-ZnO by an ultrasonic-assisted method to sensitize the room temperature gas-sensing performance of the prepared CuO/ZnO materials. The doped In₂O₃ could effectively improve the gas-sensing properties of the prepared materials to nitrogen oxides (NO_x) at room temperature. The 1% In₂O₃ doped CuO/ZnO sample (1 wt% In₂O₃-CuO/ZnO) showed the best gas-sensing properties whose response to 100 ppm NO_x reached 82%, and the detectable minimum concentration reached 1 ppm at room temperature. The prepared materials had a good selectivity, better response, very low detection limit, and high sensitivity to NO_x gas at room temperature, which would have a great development space in the gas sensor field and a great research value.

1. Introduction

In recent years, environmental monitoring gas sensors have attracted great attention. Gas sensors can detect various inflammable, explosive, toxic, and harmful gases accurately and effectively. The development of efficient, low cost, highly sensitive, highly selective and convenient chemical sensors can precisely recognize and measure the presence of toxic gases and human exposure levels, which have become a significant

endeavour for the well-being and welfare of people, safety and process control in industrial applications [1]. As gas-sensing materials, metal oxide semiconductors (MOS) have promising applications in monitoring air pollution, detecting toxic/explosive gases etc. which have been widely investigated, and have become a hotspot [2,3]. The metal oxide-based gas sensors are used widely for the detection of toxic gaseous species not only because of their superior thermal and physical stability but also due to their ability to detect very low gas concentrations [4]. Many attempts have been made to enhance the sensitivity or selectivity of oxide nanomaterials by surface modification, metal-doping, loading and the use of core shell structures [5–7].

Among various kinds of developed oxide gas-sensing materials, ZnO has attracted great attention. ZnO is a functional n-type semiconductor, which has been considered as an essential semiconductor gas-sensing material because of its high chemical stability, suitability to doping, harmlessness and economic nature [8,9]. However, pure ZnO has some inherent disadvantages, including low sensitivity, high working temperature, long response and recovery time etc. which may prevent its further development [10]. Micro/nanostructured MOS have received much attention because they have high sensitivity to small concentration of gases, low fabrication cost, long-term stability and low power consumption [11]. It is known that the morphology has a great influence on the gas-sensing properties of materials, and current researches are focused on obtaining special morphology and structure of ZnO nanomaterials by different means. Lots of different morphological ZnO and ZnO-based composite have been prepared, such as ZnO nanoflakes [12], ZnO nanowires [13], ZnO micro-flowers [14], porous ZnO micro-sheets [15], ZnO-decorated Fe₂O₃ [16] and so on.

CuO is a p-type semiconductor with a low band gap of 1.2–2.0 eV, and its p-type characteristic provides a route to form p–n junctions with n-type metal oxides [17]. CuO has been used successfully to detect H₂S using a range of p–n composite nanostructures [18–20]. Composite type sensor using two or multiple oxide material in single or multiple layers is an effective way to enhance the selectivity of the sensors. Various authors have reported selective and sensitive gas-sensing characteristics of composite oxide material. ZnO and CuO composites have been reported in gas sensing. Combination of one-dimensional ZnO and CuO microstructure may also exhibit enhanced gas-sensing property [18,21]. Rai *et al.* [22] reported the modulation of ZnO nanorod electronic properties through CuO nanoparticles and the use of functionalized ZnO nanorods for CO sensing applications. A wet chemical technique was used to prepare CuO-doped ZnO semiconductor nanomaterials with nearly controlled rod shape structure [23].

The gas-sensing properties of materials are closely related with the density and species of surface adsorptive gases. Therefore, for high performances of gas-sensitive materials they need to have a larger Brunauer–Emmett–Teller (BET) surface area. Late *et al.* [24] presented a comprehensive overview of recent developments in the application of two-dimensional (2D) layered inorganic nanomaterials as sensors, and they did a lot of works in the 2D layered sensor materials field which included the large-area MoS₂ sheets gas sensor [25], 2D WS₂-based sensor [26,27], single-layer MoSe₂-based gas sensor [28], SnSe₂ nanosheets sensor [29] and 2D black phosphorus sensor [30,31]. Porous materials have a much bigger BET surface area and much stronger gas adsorption ability, which greatly improve the gas-sensing performance of the porous materials. Porous ZnO nano/microstructures have also drawn extensive research attention. Specifically, the introduction of pores into ZnO nano/microstructures facilitates the gas diffusion and mass transport, enormously improving gas sensor performance [32]. Liu *et al.* [33] reported the synthesis of three-dimensional hierarchical ZnO porous structures functionalized by Au. Wang *et al.* [34] reported a facile approach to prepare nest-like three-dimensional porous ZnO with hierarchically 2D lamellar structures. The nest-like ZnO hierarchically porous structures displayed a superior gas-sensing performance. Liu *et al.* [35] reported the synthesis of single-crystalline porous ZnO nanosheets by annealing ZnS (ethylenediamine) complex precursor, which exhibited highly sensitive performance. Huang *et al.* [36] reported tunable macro–mesoporous ZnO (M/m-ZnO) nanostructures, and the prepared M/m-ZnO nanostructures demonstrated better ethanol and acetone sensing properties. Template and template-free mesoporous ZnO-based structures have been widely prepared as gas materials [37].

In this study, ordered mesoporous ZnO nanoparticles have been synthesized by a template method. The electroplating after chemical plating method was creatively used to form copper film on the porous ZnO surface, and then a CuO film-decorated ordered porous ZnO composite (CuO film–ZnO) was obtained by a high-temperature oxidation method. In₂O₃ was loaded in the prepared CuO film–ZnO by ultrasonic-assisted method to sensitize the room temperature gas-sensing performance of the prepared materials. The fluffy porous structure was helpful for gas diffusion and surface reaction, which led to the sensor exhibiting faster response. The copper film was more uniform when the electroplating after

chemical plating method was used to form copper film, and the n–p heterojunction between CuO film and ZnO matrix played an important role in the enhancement of the sensor response and selectivity. The In_2O_3 played a sensitizer role to sensitize the surface reaction. In_2O_3 was a catalyst, it reduced the activation energy of the oxidation–reduction reaction on the surface of composites, efficiently separated the oxygen molecules, improved the activity of gas-sensitive materials, increased the free electron amount and expedited the reaction rate. As such, the gas sensitivity of the composites was enhanced. The prepared material greatly reduced the working temperature of the sensor, which would have a great development prospect and great research value in the sensor field.

2. Experimental

2.1. Materials

All chemicals used in our work were of analytical grade, and used without any further purification. Cetyltrimethylammonium bromide (CTMAB, A.R.) was purchased from Changzhou Xinhua Reagent Research Institute in China. $\text{Zn}(\text{Ac})_2 \cdot 2\text{H}_2\text{O}$ was purchased from Tianjin Guangfu Fine Chemical Research Institute in China. Sodium hydroxide (NaOH, A.R.) was purchased from Beijing Chemical Works Research Institute in China. Potassium sodium tartrate tetrahydrate ($\text{C}_4\text{H}_4\text{O}_6\text{KNa} \cdot 4\text{H}_2\text{O}$, A.R.) was purchased from Tianjin Guangfu Technology Development Co. Ltd in China. Formaldehyde solution (HCHO, A.R.) was purchased from Tianjin Fuchen Chemical Reagents Factory in China. Ethylene diamine tetraacetic acid disodium (EDTA-2Na, A.R.) was purchased from Shenyang Reagent Factory in China. Copper(II) sulfate pentahydrate ($\text{CuSO}_4 \cdot 5\text{H}_2\text{O}$, A.R.) was purchased from Sinopharm Chemical Reagent Co. Ltd in China. Ethanol and deionized water were used for all processes of washing and dissolution.

2.2. Preparation of materials

2.2.1. Preparation of mesoporous ZnO nanoparticles

One gram of CTMAB was added into 480 ml of deionized water, and the mixture was vigorously stirred until the solution was homogeneous at 80°C . About 4.92 g of $\text{Zn}(\text{Ac})_2 \cdot 2\text{H}_2\text{O}$ was dissolved into the solution with stirring. The pH of the solution was adjusted with LiOH to alkaline; the reaction then proceeded at 80°C for 2 h. The product was filtered, washed with deionized water and dried at room temperature to get the powder sample. The original sample was calcined at 500°C for 4 h, and the ordered mesoporous ZnO material was finally obtained.

2.2.2. Preparation of CuO film on the mesoporous ZnO matrix

The electroless plating solution was prepared according to table 1. The prepared ordered porous ZnO material was added into the electroless plating solution, which was reacted for 1 h under vigorous stirring. The powder was filtered, washed with deionized water and dried to afford a reddish brown powder with metallic lustre.

The prepared powder was put into semipermeable membrane, and the negative pole was inserted into the powder. The powder was immersed in the plating solution (table 2). The sheet copper was used as anode, voltage was regulated at 17 V, electricity was regulated at 1 A and the plating solution was electrified for 1 h. The powder was filtered, washed with deionized water, dried, calcined at 500°C for 4 h to afford a black CuO film–ZnO powder sample.

2.2.3. Preparation of In_2O_3 sensitization CuO film–ZnO composite material

In order to study the effect of different In_2O_3 decoration amounts on the gas-sensing performance, a series of In_2O_3 decorated CuO film–ZnO composites were synthesized. In a typical procedure, 0.1 g prepared CuO film–ZnO product was dispersed in 20 ml deionized water with the aid of ultrasonication. A certain amount of $\text{In}(\text{NO}_3)_3$ ($\text{In}(\text{NO}_3)_3$ concentration: 10 wt%, 15 wt%, 20 wt% and 25 wt%) was added in the above solution. The reaction system was dispersed in ultrasonic for 10 min, and the suspension liquid was aged for 2 h at room temperature. The suspension liquid was filtered, washed with deionized water and dried for 10 h at 60°C . The prepared samples were heated for 4 h at 500°C with a warming rate of 2°C min^{-1} to afford the products. The In-loaded contents were obtained with an inductively coupled

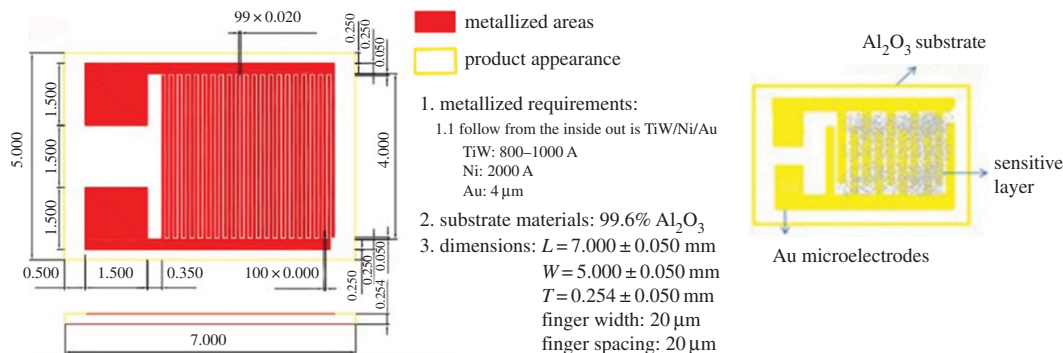


Figure 1. Parameters of interdigitated gold electrode and schematic diagram of the prepared gas sensor.

Table 1. Electroless plating solution formula.

reagents	CuSO ₄ ·5H ₂ O	HCHO	EDTA-2Na	sodium potassium tartrate	potassium ferrocyanide	dipyridyl	NaOH
concentration	25 g l ⁻¹	20–40 g l ⁻¹	20–40 g l ⁻¹	10–20 g l ⁻¹	10 mg l ⁻¹	10 mg l ⁻¹	20%

Table 2. Plating solution formula.

reagents	CuSO ₄ ·5H ₂ O	NaOH	citric acid	sodium potassium tartrate	deionized water
amount	13 g	31.25 g	50 g	10 g	250 ml

plasma–optical emission spectrometer (ICAP 6000 Series), and the corresponding doping contents of In₂O₃ were calculated which were 0.5, 1, 3 and 6 wt%, respectively.

2.3. Characterization

Powder X-ray diffraction (XRD) patterns were collected with a Siemens D5005 diffractometer using Cu–K α radiation ($\lambda = 1.5418$ Å and operating at 30 kV and 20 mA). Transmission electron microscopy (TEM) images were taken with a JEOL 2010 TEM instrument. The scanning electron microscopy (SEM) images were taken with a JEOL JSM-5600 L. Physical adsorption of nitrogen was performed with a Micromeritics ASAP2010M volumetric adsorption analyser at 77 K. A sample was degassed in vacuum at 573 K for 12 h before measurement. Surface area was calculated based on the BET model, while pore size was computed using the Barrett–Joyner–Halenda method.

2.4. The preparation of gas sensor

In this study, an interdigitated Au electrode was selected for the gas-sensing detection. The sample was disposed as follows: about 3 mg of the prepared sample was dispersed in ethanol, which was dispersed ultrasonically for about 20 min. The sample material was spin-coated on the interdigitated electrode surface to form a thin film, which was dried to obtain the gas sensor. The parameters of interdigitated gold electrode and schematic diagram of the prepared gas sensor are shown in figure 1.

The sensor was welded onto a socket, and the electrical properties of the sensor were measured by a JF02E intelligent gas-sensing analysis system. The sensor response was defined as

$$S(\%) = \left[\frac{(R_a - R_g)}{R_a} \right] \times 100\%. \quad (2.1)$$

Here, R_a and R_g were the resistances of the sensors in the air and target gas, respectively. The response and recovery time were defined as the time taken by the sensors to achieve 85% of the total resistance change in the case of adsorption and desorption, respectively [38–40].

3. Results and discussion

3.1. Structure and morphology

Figure 2 shows the wide-angle XRD pattern of the prepared ordered mesoporous 1 wt% In_2O_3 -CuO/ZnO sample. The sharp diffraction peaks indicated the highly crystalline characteristic of 1 wt% In_2O_3 -CuO/ZnO samples. All of the diffraction peaks were consistent with the standard card of CuO (JCPDS No. 44-0706), which showed that the CuO has been deposited on the surface of the ZnO. The diffraction peaks of wurtzite ZnO (JCPDS No. 36-1451) could be seen in the prepared material. In the XRD pattern, the characteristic peaks of the In_2O_3 could also be seen. It showed that the In_2O_3 has been doped into the prepared CuO film-ZnO matrix material.

Figure 3 shows the energy-dispersive X-ray spectra of CuO/ZnO and 1 wt% In_2O_3 -CuO/ZnO samples. From figure 3*a*, the peaks of C, Zn, O, Si and Cu could be seen in CuO/ZnO sample. The sample was first placed on a silicon wafer when the sample was tested, which led to the highest Si content peak. The C and O were mainly from the conducting resin. In figure 3*b*, the indium (In) content peaks could be seen in 1 wt% In_2O_3 -CuO/ZnO sample, which could prove the existence of the In_2O_3 in 1 wt% In_2O_3 -CuO/ZnO sample, and the In_2O_3 has been successfully assembled into the CuO film-ZnO matrix. The Pt content peak was attributed to the Pt conductive agent sprayed on the surface of the sample. There were no peaks of other elements in samples, which indicated that the prepared samples were pure.

Figure 4 shows the SEM image of CuO film-ZnO and 1 wt% In_2O_3 -CuO/ZnO samples. From figure 4*a*, the CuO/ZnO sample showed a whole flower-like appearance, whose surface was smooth. From figure 4*b*, the 1 wt% In_2O_3 -CuO/ZnO sample showed an analogous flower-like structure, which obtained from the petals of flower-like CuO/ZnO sample fallen off, the analogous flower-like structures were heaped with irregular flaky grain.

Figure 5*a* shows the TEM image of the 1 wt% In_2O_3 -CuO/ZnO sample, which was taken parallel to the direction of the channels. From figure 5*a*, it could be seen that there were a lot of ordered pores in the sample. Figure 5*b* shows the high-resolution TEM (HRTEM) image of the 1% In_2O_3 -CuO/ZnO sample. From figure 5*b*, it could be seen that the lattice fringes of the sample were very clear, which were the lattice fringes of CuO. In the HRTEM images, the ordered pores could be very clearly seen under the CuO lattice fringes, which indicated that the CuO thin films were formed on the surface of the prepared sample.

3.2. Gas-sensing performance

Figure 6*a* shows the gas response bar charts of different In_2O_3 -doped concentration samples to different concentrations of NO_x . The study found that the sensitivity of each sample decreased when NO_x concentration decreased from 100 to 5 ppm. The results showed that In_2O_3 could significantly enhance the response of the materials to NO_x , and the 1 wt% In_2O_3 -CuO/ZnO sample had the best response to NO_x among five prepared (0, 0.5, 1, 3, 6 wt%) In_2O_3 -CuO/ZnO sensor samples in this study. At room temperature, the response and response time of the sensors with different In_2O_3 contents to 100 ppm NO_x gas are shown in the electronic supplementary material, table S1.

Under the current operating conditions, the response-recovery curves of 1 wt% In_2O_3 -CuO/ZnO sensor are shown in figure 6*b*. The resistance sharply decreased when the NO_x gas was injected, and the resistance recovered to its initial value when the NO_x gas was discharged. When the prepared sensor was in air, oxygen molecules were adsorbed on the surface of the sensor; the adsorbed oxygen captured electrons from the conductance band to produce negatively charged oxygen species. These chemisorbed oxygen species would act as surface acceptors, trapping electrons and increasing surface resistance of the sensor. When the NO_x gas was injected, the NO_x would react with the formed oxygen ions, which released the trapped electrons back to the sensor surfaces, and the resistance of the sensor was sharply decreased. It indicated that the prepared sensing material was a p-type semiconductor material.

Figure 6*c* shows the response and response time curve of the 1 wt% In_2O_3 -CuO/ZnO sample to 100–1 ppm NO_x at room temperature. When the NO_x gas was injected into the sensing chamber, the resistance of the 1 wt% In_2O_3 -CuO/ZnO sensor rapidly decreased, and reached the minimum resistance value in a short time. The 1 wt% In_2O_3 -CuO/ZnO sensor exhibited a fast and reversible response to NO_x , the response time being only 7 s to 100 ppm NO_x which was much shorter than that reported in a lot of literature [26,39,41–43], and the corresponding response reached up to 82%. The responses were weakened with the reduction in the NO_x concentration from 100 to 1 ppm, and the corresponding response time increased. It was related to the gas concentration, gas diffusion and adsorption on the

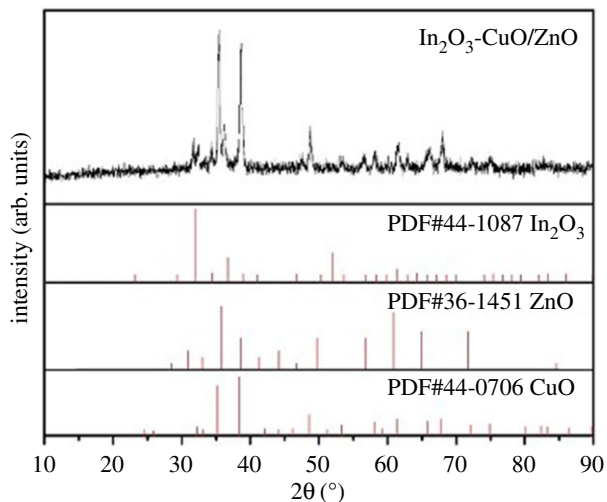


Figure 2. Wide-angle XRD pattern of the 1 wt% $\text{In}_2\text{O}_3\text{-CuO/ZnO}$ sample.

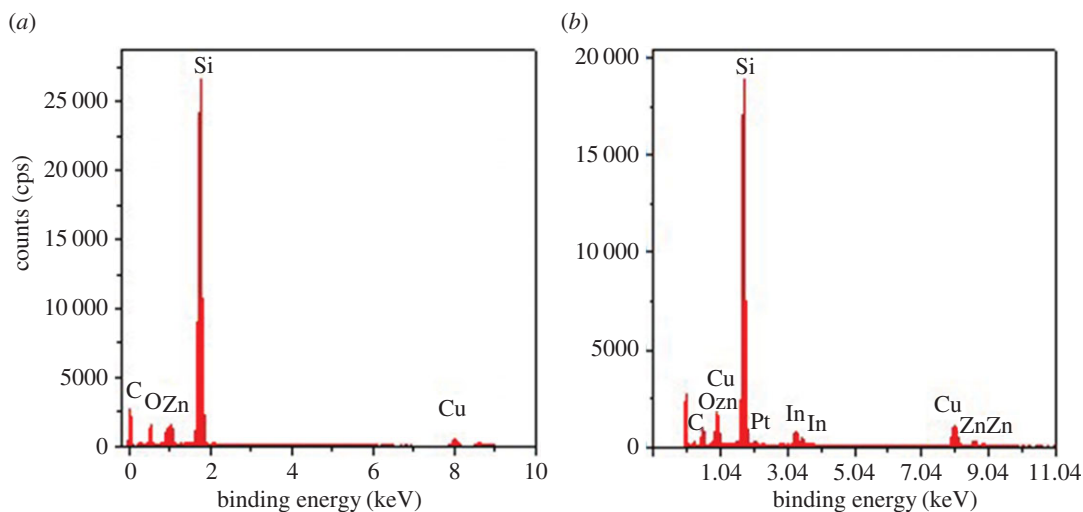


Figure 3. Energy-dispersive X-ray spectra of the (a) CuO/ZnO sample and (b) 1 wt% $\text{In}_2\text{O}_3\text{-CuO/ZnO}$ sample.

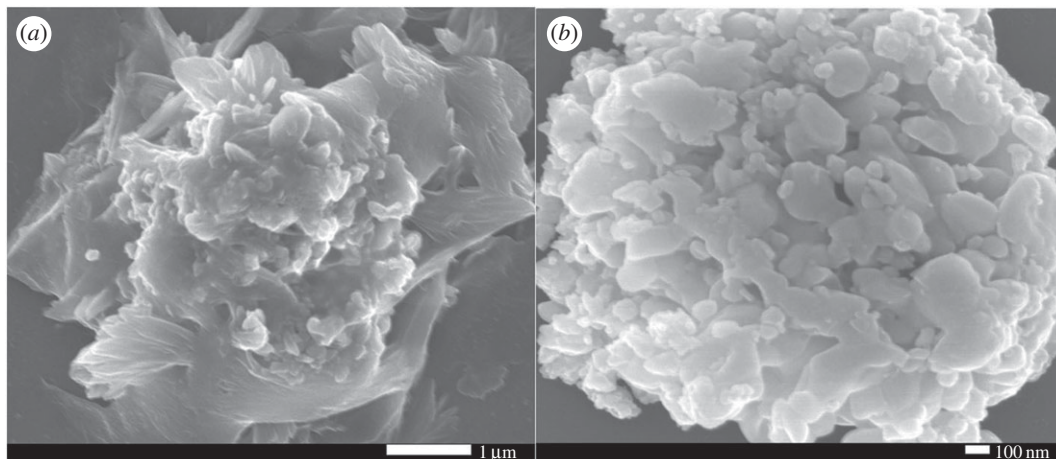


Figure 4. SEM images of the (a) CuO/ZnO and (b) 1% $\text{In}_2\text{O}_3\text{-CuO/ZnO}$ sample.

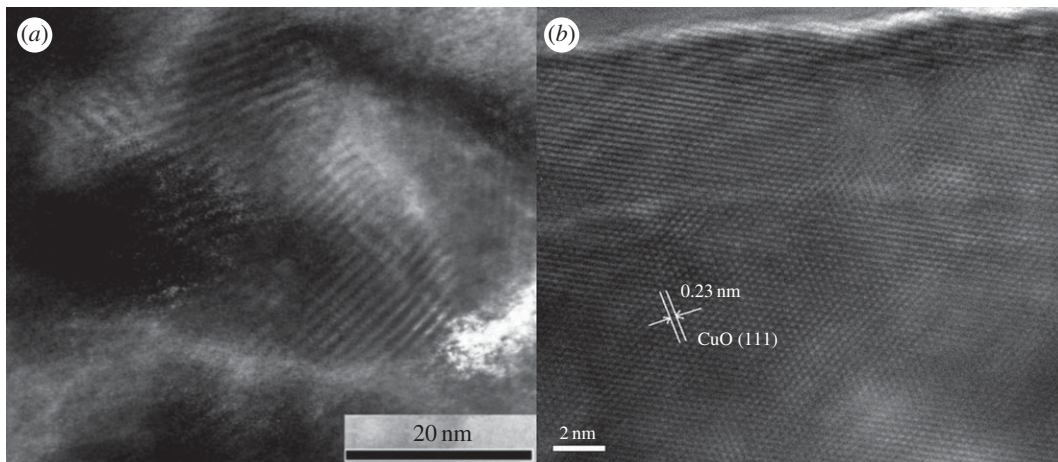


Figure 5. (a) TEM image and (b) HRTEM image of the 1 wt% $\text{In}_2\text{O}_3\text{-CuO/ZnO}$ sample.

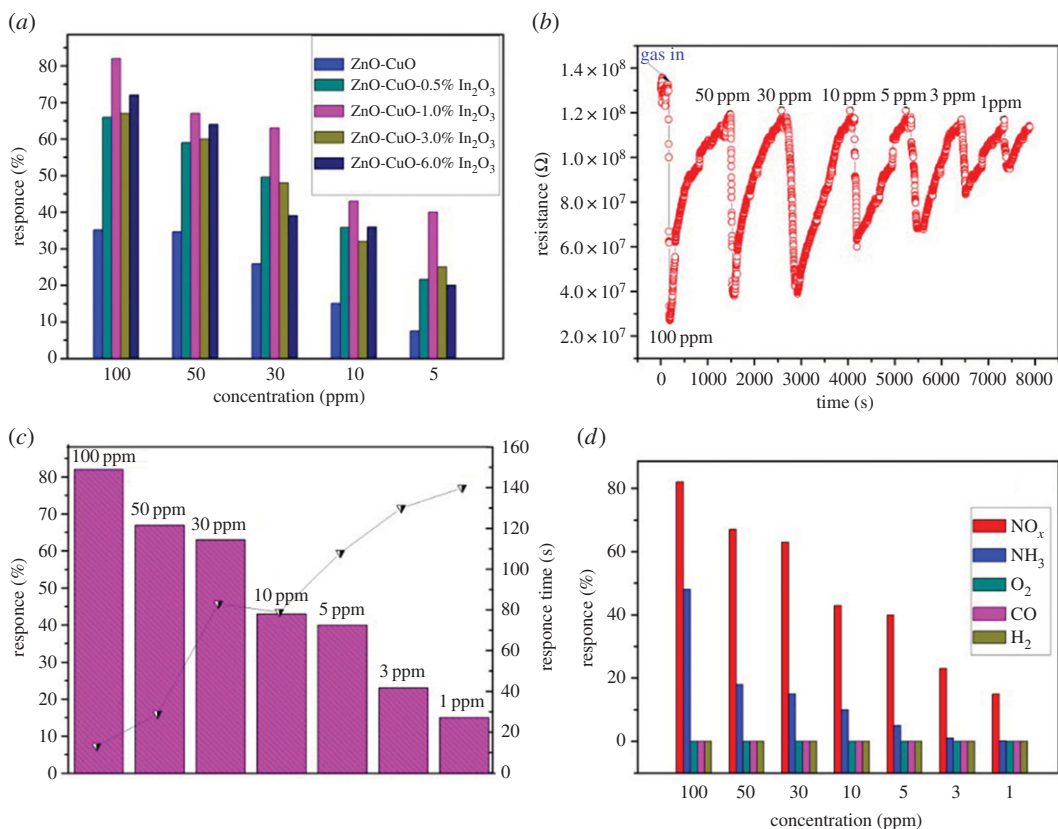


Figure 6. (a) Gas response bar charts of different In_2O_3 -doped concentration samples to different concentrations of NO_x ; (b) dynamic response–recovery curves of 1 wt% $\text{In}_2\text{O}_3\text{-CuO/ZnO}$ sample; (c) response and response time curve of the 1 wt% $\text{In}_2\text{O}_3\text{-CuO/ZnO}$ sample to different concentrations of NO_x ; (d) gas response bar charts of 1 wt% $\text{In}_2\text{O}_3\text{-CuO/ZnO}$ sample to 100 ppm different gases.

surface of the nanomaterials. With decreasing of NO_x concentration, the NO_x gas partial pressure declined in the reaction chamber which led to gas phase reaction velocity being slower, and the response time increased. It is worth noting that the minimum detection limit of 1 wt% $\text{In}_2\text{O}_3\text{-CuO/ZnO}$ gas sensor was only 1 ppm at room temperature, the corresponding response still reached 17% and the corresponding response time was 136 s.

In order to study the selectivity of 1 wt% $\text{In}_2\text{O}_3\text{-CuO/ZnO}$ gas sensor, the responses of 1 wt% $\text{In}_2\text{O}_3\text{-CuO/ZnO}$ sensor to different gases (NO_x , NH_3 , O_2 , CO and H_2) were measured at room temperature. The corresponding test results are shown in figure 6d. The 1 wt% $\text{In}_2\text{O}_3\text{-CuO/ZnO}$ gas sensor had a

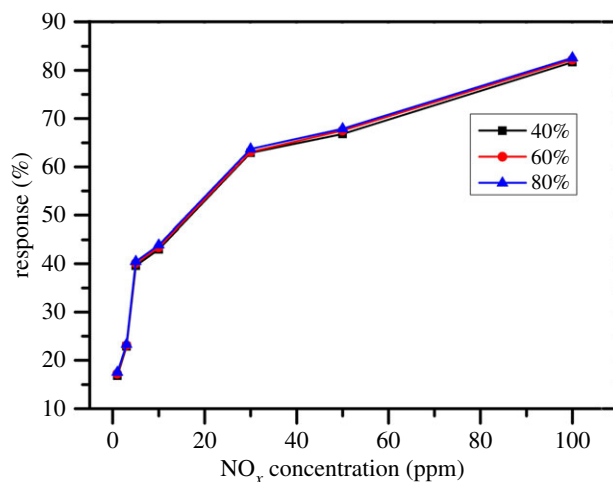


Figure 7. Influence of the humidity on the gas responses of 1 wt% $\text{In}_2\text{O}_3\text{-CuO/ZnO}$ sample.

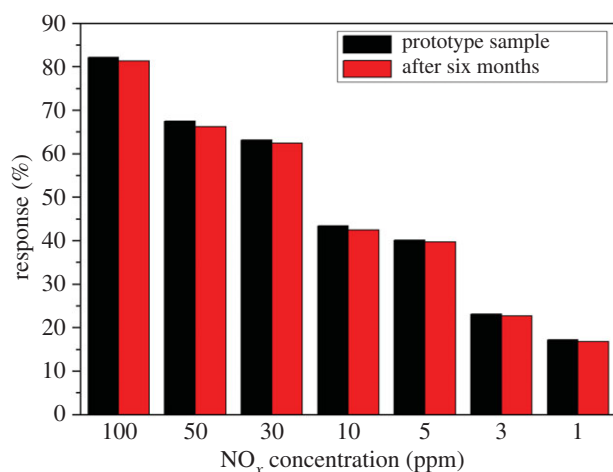


Figure 8. Stability bar charts of 1 wt% $\text{In}_2\text{O}_3\text{-CuO/ZnO}$ sample.

relatively high response to NH_3 . When the NH_3 concentration was 100 ppm, the response reached 48%. However, the response to NH_3 of the sensor was also significantly lower than the response to the same concentration of NO_x . The response of other gases (O_2 , CO and H_2) was closer to 0%. The experimental results showed that the 1 wt% $\text{In}_2\text{O}_3\text{-CuO/ZnO}$ gas sensor had good selectivity.

The humidity is one of the significant factors in the gas-sensing process, and the degree of humidity influences the sensing performance of oxide semiconductors. However, the humidity has little effect on NO_x gas response in this study. The result is shown in figure 7.

Figure 8 shows the stability bar charts of 1 wt% $\text{In}_2\text{O}_3\text{-CuO/ZnO}$ sample. The response of the prepared sample remained stable after six months. It indicated that the prepared 1 wt% $\text{In}_2\text{O}_3\text{-CuO/ZnO}$ sample had good stability.

3.3. Discussion of sensing mechanism

The gas-sensing behaviour of ZnO results from the surface chemical reactions. The reactants are the chemisorbed oxygen species (O^- , O_2^- and O^{2-}) and the adsorbed target gas molecules. These reactions lead to the resistance variation of the gas sensor. Generally, the n-type oxide semiconductor materials (such as ZnO) response mechanism involves the interaction between the detected gases and chemisorbed oxygen ions on the surface of the materials, leading to the resistance change of the sensor [44,45]. In air, the oxygen molecules adsorb on the surface of the materials, which can capture free electrons from the materials to form negative oxygen ions (O^{2-} , O^- and O_2^-) at grain boundaries, and a thick space charge

layer will be formed. The negative surface charges will generate a higher surface potential barrier, which leads to a high electrical resistance [46,47]. The process can be expressed as follows:



When the sensor is exposed in oxidizing NO_x gas, the NO_x gases attract the electrons from sensor materials, which can be attributed to their high electron affinity. The process leads to electrons of the sensor materials transferring to the surface NO_x , and forming NO_2^- (from NO_2) and NO^- (from NO). The process traps electrons from the conduction band or donor level of materials, which leads to electron density reduction and the hole carrier density increase in the sensor. The hole carriers result in a decrease in resistance of the semiconductor layer. It will lead to a thinner space-charge layer, and reduce the potential barrier at the grain boundaries and cause a decrease in the sensor resistance [39]. The process can be expressed as follows:



Also, the target gases NO_2 and NO directly adsorb on the sensor, which react with O^- and generate bidentate NO_3^- (s) and NO_2^- , and release the trapped electrons back into the conduction band. The process can be expressed as follows [48]:



The band gap (E_g) of ZnO is 3.4 eV, and its electron affinity (χ) is 4.35 eV. The band gap of CuO is 1.35 eV, and its electron affinity is 4.07 eV. From a thermodynamic perspective, the electrons will transfer from the conduction band of CuO to ZnO, while the holes will oppositely migrate from the valence band of ZnO to CuO [49]. The process will increase the charge separation rate of electron-hole pairs under the bias potential, while the longer lifetime of electron-hole pairs of CuO/ZnO will be attributed to the formation of the p-n heterojunction. The p-n heterojunction may facilitate the adsorption of gas molecules. Thus, CuO/ZnO composite shows a higher sensing activity than pure ZnO, the pure ZnO has no gas response at room temperature. However, the formation of a p-n junction results in higher resistance [22].

The higher sensitivity of CuO/ZnO composite can be attributed to the electronic sensitization induced by CuO [50,51]. There are more active sites and more chemisorbed oxygen species on the surface of p-type semiconductors than n-type semiconductors [51,52]. The modified CuO nanostructures can act as a strong acceptor of electrons from ZnO [50]. The Fermi energy levels of n-type ZnO and p-type CuO are equalized which is due to the charge transfer [53,54]. The introduction of CuO film on the surface of the porous ZnO increases the carrier density of the ZnO, which results in the electron redistribution between the ZnO and the CuO [55]. In the air, oxygen molecules capture electrons from CuO, and chemisorbed oxygen species are formed on its surface [56]. Meanwhile, electrons transfer from ZnO to CuO, which causes the formation of an electron depletion layer (EDL) extending into ZnO [51]. The EDL significantly narrows the conducting part and dominates the conductivity of CuO/ZnO [57,58]. The decoration of CuO promotes the chemisorption of oxygen species and the chemical reactions on the surface of CuO/ZnO [51,59]. This leads to an enhancement in the sensitivity of CuO/ZnO composite [60].

In addition, high specific surface area of sensing material usually has positive effects on the sensing response [61]. The porous structure helps to increase the gas-sensing performance. The porous structure provides abundant pores, which is more beneficial to diffusion of gas molecules [62,63]. Moreover, it also provides more active sites, and improves the kinetics of chemical reactions on the surface [63]. This also results in enhanced sensing performance. Furthermore, there would be more oxygen species chemisorbed on the surface of CuO film structures due to its large surface to volume ratio [64]. Thus, the sensitivity of the CuO/ZnO composite is further enhanced. In this study, CuO is introduced onto the surface of ordered mesoporous zinc oxide by electrodeposition after chemical deposition method. The active site density is improved by the advantages of porous and large specific surface area of mesoporous materials. CuO is dispersed on the porous surface of the mesoporous ZnO matrix material to provide an effective gas diffusion channel for CuO contacting with the gas. The provided multiple active sites make NO_x easier to react with adsorbed oxygen ions on the surface, which increases gas sensitivity performance.

On the surface of the prepared CuO/ZnO composite, the heterogeneous structure can be formed between CuO and ZnO by ultrasonic method, and the gas-sensitive properties can be enhanced by In_2O_3 . Generally, the n-n (or p-n) type heterojunction-based interfacial barriers between In_2O_3 and ZnO (or

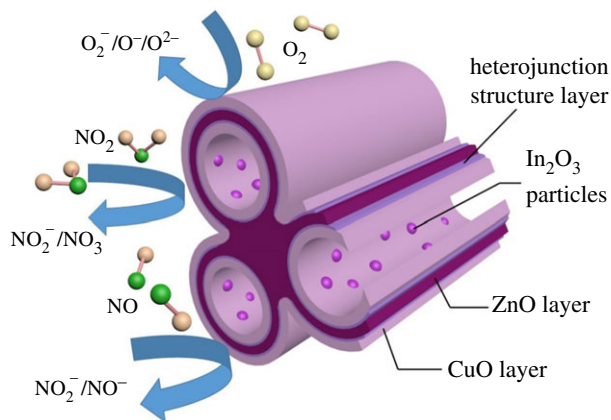


Figure 9. A schematic diagram of sensing mechanism of 1 wt% In_2O_3 -CuO/ZnO sensor.

CuO) nanocrystals are another mechanism accounting for the enhanced sensing performance [45,65–67]. In this study, the doping content is very little which forms discontinuity phase. A possible gas-sensing mechanism is as follows: in the band of interfaces, there is a spike at the In_2O_3 side along with a notch at the host side. The discontinuity band sets barriers for electrons in both conduction band and valence band. The heterojunction interfacial barriers can strongly modify the charge transport behaviours of carriers because the carrier concentration varies exponentially with the barrier height. Further studies are required to determine the mechanism through which the In_2O_3 -doped semiconductor interfacial barriers promote the sensing performance towards gases [68]. Also, the catalysis of the In_2O_3 should not be overlooked. The catalytic activity of In_2O_3 accelerates the dissociation of oxygen molecules, and causes a spillover of the adsorbed oxygen ions on the surface of 1% In_2O_3 -CuO/ZnO composite. More adsorbed oxygen ions provide more sensing activity sites and shows high response [45,69–71]. In this study, the doped quantity In_2O_3 is very little, the p-n heterojunction or n-n/p-p homo-type heterojunction cannot be formed, and the In_2O_3 only plays a role of sensitizer to sensitize the surface reaction. With the In_2O_3 content increasing, the sensitization is enhanced. But, the sensitized mechanism is changed when the doped In_2O_3 quantity exceeded the limit, which can be explained with heterojunction mechanism, and the response of the sensor will be the lower when the In_2O_3 content is not enough to form the continuous heterojunction.

In this study, the remarkable gas-sensing performance of the prepared 1 wt% In_2O_3 -CuO/ZnO sensor may be for the following reasons. First, the fluffy porous structure is helpful for gas diffusion and surface reaction, which lead to the sensor exhibiting faster response. Second, n-p heterojunction between CuO and ZnO plays an important role in the enhancement of the sensor response and selectively. The CuO has a lower Fermi level than ZnO, and ZnO would receive electrons from CuO, leading to the formation of an accumulation layer at the CuO/ZnO interface. The increase in electrons on the surface of ZnO is able to facilitate adsorption of oxygen molecules and a decrease in resistance. Third, the doping of In_2O_3 is also helpful for remarkable gas-sensing performance of 1 wt% In_2O_3 -CuO/ZnO composite. The reasons include electron interactions between In_2O_3 and ZnO, the catalytic activity of In_2O_3 accelerates the dissociation of oxygen molecules, and causes a spillover of the adsorbed oxygen ions on the surface of 1 wt% In_2O_3 -CuO/ZnO composite. More adsorbed oxygen ions provide more sensing sites, and show high response. The mechanism is intuitively explained in figure 9.

4. Conclusion

An ordered mesoporous ZnO nanomaterial has been synthesized by a template method. The prepared porous ZnO nanomaterial is used as matrix to prepare a porous Cu film-ZnO composite by the electroplating after chemical plating method, and finally a CuO film-decorated ordered porous ZnO composite is obtained by a high-temperature oxidation method. Then, In_2O_3 is loaded into the prepared CuO/ZnO by an ultrasonic-assisted method, affording an In_2O_3 -CuO/ZnO composite. The prepared 1 wt% In_2O_3 -CuO/ZnO composite shows the best gas-sensing performance, in which the In_2O_3 doping content is only 1 wt%. For 1 wt% In_2O_3 -CuO/ZnO sample, its response time is only 7 s to 100 ppm NO_x , and the corresponding response reaches 82%. It is worth noting that the minimum detection limit of

1 wt% In₂O₃–CuO/ZnO gas sensor was only 1 ppm at room temperature, the corresponding response still reached 17% and the corresponding response time was 136 s. The response of the 1 wt% In₂O₃–CuO/ZnO gas sensor is much higher, the minimum detection limit is much lower, the selectivity and stability are much better and the corresponding response time is much shorter at room temperature than that reported in a lot of literature.

Data accessibility. All relevant data are within the paper and the electronic supplementary material files.

Authors' contributions. T.-t.L. wrote the manuscript. N.B. conducted the experiments. A.-f.G. revised the manuscript. H.Y. conceived and designed the project. Y.Y. and X.-t.D. discussed the results and sensing mechanism. All authors gave final approval for publication.

Competing interests. We declare we have no competing interests.

Funding. We gratefully acknowledge the support of the work by the National Natural Science Foundation of China (grant no. 51572034), the National Natural Science Foundation of China (grant no. 21601018) and the National Natural Science Foundation of Changchun University of Science and Technology (no. XQNJJ-2015-07).

References

- Kimura M, Sakai R, Sato S, Fukawa T, Ikehara T, Maeda R, Mihara T. 2012 Sensing of vaporous organic compounds by TiO₂ porous films covered with polythiophene layers. *Adv. Funct. Mater.* **22**, 469–476. (doi:10.1002/adfm.201101953)
- Rai P, Raj S, Ko KJ, Park KK, Yu YT. 2013 Synthesis of flower-like ZnO microstructures for gas sensor applications. *Sens. Actuat. B Chem.* **178**, 107–112. (doi:10.1016/j.snb.201212031)
- Flak D, Braun A, Mun BS, Park JB, Parlinska-Wojtan M, Graule T, Rekas M. 2013 Spectroscopic assessment of the role of hydrogen in surface defects, in the electronic structure and transport properties of TiO₂, ZnO and SnO₂ nanoparticles. *Phys. Chem. Chem. Phys.* **15**, 1417–1430. (doi:10.1039/C2CP42601C)
- Kim NH, Choi SJ, Yang DJ, Bae J, Park J, Kim ID. 2014 Highly sensitive and selective hydrogen sulfide and toluene sensors using Pd functionalized WO₃ nanofibers for potential diagnosis of halitosis and lung cancer. *Sens. Actuat. B Chem.* **193**, 574–581. (doi:10.1016/j.snb.201312011)
- Katoch A, Choi SW, Sun GJ, Kim SS. 2013 An approach to detecting a reducing gas by radial modulation of electron depleted shells in core shell nanofiber. *J. Mater. Chem. A* **43**, 13 588–13 596. (doi:10.1039/C3TA13087H)
- Katoch A, Sun GJ, Choi SW, Hishita S, Kulish VV, Wu P, Kim SS. 2014 Acceptor compensated charge transport and surface chemical reactions in Au-implanted SnO₂ nanowires. *Sci. Rep.* **4**, 4622–4629. (doi:10.1038/srep04622)
- Wan GX, Ma SY, Li XB, Li FM, Bian HQ, Zhang LP, Li WQ. 2014 Synthesis and acetone sensing properties of Ce-doped ZnO nanofibers. *Mater. Lett.* **114**, 103–106. (doi:10.1016/j.matlet.201309094)
- Mani GK, Rayappan JBB. 2015 A highly selective and wide range ammonia sensor—nanostructured ZnO: Co thin film. *Mater. Sci. Eng. B* **191**, 41–50. (doi:10.1016/j.mseb.2014.10.007)
- Fu YM, Zhao YY, Wang PL, Xing LL, Xue XY. 2015 High response and selectivity of a Cu–ZnO nanowire nanogenerator as a self-powered/active H₂S sensor. *Phys. Chem. Chem. Phys.* **17**, 2121–2126. (doi:10.1039/C4CP04983G)
- Tabassum R, Mishra SK, Gupta BD. 2013 Surface plasmon resonance-based fiber optic hydrogen sulphide gas sensor utilizing Cu–ZnO thin films. *Phys. Chem. Chem. Phys.* **15**, 11 868–11 874. (doi:10.1039/C3CP51525G)
- Cai XY, Hu D, Deng SJ, Han BQ, Wang Y, Wu JM, Wang YD. 2014 Isopropanol sensing properties of coral-like ZnO–CdO composites by flash preparation via self-sustained decomposition of metal–organic complexes. *Sens. Actuat. B Chem.* **198**, 402–410. (doi:10.1016/j.snb.201403093)
- Kaneti YV, Yue J, Jiang X, Yu A. 2013 Controllable synthesis of ZnO nanoflakes with exposed (1010) for enhanced gas sensing performance. *J. Phys. Chem. C* **117**, 13 153–13 162. (doi:10.1021/jp404329q)
- Park SH, An S, Ko HS, Jin CY, Lee CM. 2012 Synthesis of nanograin ZnO nanowires and their enhanced gas sensing properties. *ACS Appl. Mater. Interfaces* **4**, 3650–3656. (doi:10.1021/am300741r)
- Huang JR, Wu YJ, Gun CP, Zhai MH, Yu K, Yang M, Liu JH. 2010 Preferential growth of long ZnO nanowires and its application in gas sensor. *Sens. Actuat. B Chem.* **146**, 206–212. (doi:10.1016/j.snb.201211044)
- Wang LW, Wang SR, Zhang HX, Wang YH, Yang JD, Huang WP. 2014 Au-functionalized porous ZnO microspheres and their enhanced gas sensing properties. *New J. Chem.* **38**, 2530–2537. (doi:10.1039/C3NJ01562A)
- Kaneti YV, Zakaria QMD, Zhang Z, Chen C, Yue J, Liu M, Jiang X, Yu A. 2014 Solvothermal synthesis of ZnO-decorated α -Fe₂O₃ nanorods with highly enhanced gas-sensing performance toward n-butanol. *J. Mater. Chem. A* **2**, 13 283–13 292. (doi:10.1039/C4TA01837K)
- Mashock M, Yu KH, Cui SM, Mao S, Lu GH, Chen JH. 2012 Modulating gas sensing properties of CuO nanowires through creation of discrete nanosized p–n junctions on their surfaces. *ACS Appl. Mater. Interfaces* **4**, 4192–4199. (doi:10.1021/am300911z)
- Kim JY, Kim WS, Yong KJ. 2012 CuO/ZnO heterostructured nanorods: photochemical synthesis and the mechanism of H₂S gas sensing. *J. Phys. Chem. C* **116**, 15 682–15 691. (doi:10.1021/jp302129j)
- Sun GJ, Choi SW, Katoch A, Wu P, Kim SS. 2013 Bi-functional mechanism of H₂S detection using CuO–SnO₂ nanowires. *J. Mater. Chem. C* **35**, 5454–5462. (doi:10.1039/C3TC30987H)
- Park S, Park S, Jung J, Hong T, Lee S, Kim HW, Lee C. 2014 H₂S gas sensing properties of CuO-functionalized WO₃ nanowires. *Ceram. Int.* **40**, 11 051–11 056. (doi:10.1016/j.ceramint.201403120)
- Wang JX, Sun XW, Yang Y, Kyaw KKA, Huang XY, Yin JZ, Wei J, Demir HV. 2011 Free-standing ZnO–CuO composite nanowire array films and their gas sensing properties. *Nanotechnology* **22**, 325704. (doi:10.1088/0957-4484/22/32/325704)
- Rai P, Jeon SH, Lee CH, Lee JH, Yu YT. 2014 Functionalization of ZnO nanorods by CuO nanospikes for gas sensor applications. *RSC Adv.* **4**, 23604–23609. (doi:10.1039/c4ra00078a)
- Rahman MM, Asiri AM. 2015 Development of selective and sensitive bicarbonate chemical sensor based on wet-chemically prepared CuO–ZnO nanorods. *Sens. Actuat. B Chem.* **214**, 82–91. (doi:10.1016/j.snb.2015.02.113)
- Kannan PK, Late DJ, Morgan H, Rout CS. 2015 Recent developments in 2D layered inorganic nanomaterials for sensing. *Nanoscale* **7**, 13293–13312. (doi:10.1039/C5NR03633J)
- Late DJ *et al.* 2013 Sensing behavior of atomically thin-layered MoS₂ transistors. *ACS Nano* **7**, 4879–4891. (doi:10.1021/nn400026u)
- Late DJ, Kanawade RV, Kannan PK, Rout CS. 2016 Atomically thin WS₂ nanosheets based gas sensor. *Sens. Lett.* **14**, 1249–1254. (doi:10.1166/sl.2016.3764)
- Pawbake AS, Waykar RG, Late DJ, Jadhkar SR. 2016 Highly transparent wafer-scale synthesis of crystalline WS₂ nanoparticle thin film for photodetector and humidity-sensing applications. *ACS Appl. Mater. Interfaces* **8**, 3359–3365. (doi:10.1021/acsami.5b11325)
- Late DJ, Doneux T, Bougouma M. 2014 Single-layer MoSe₂ based NH₃ gas sensor. *Appl. Phys. Lett.* **105**, 233103. (doi:10.1063/1.4903358)
- Pawar M, Kadam S, Late DJ. 2017 High-performance sensing behavior using electronic ink of 2D SnS₂ nanosheets. *Chem. Select* **2**, 4068–4075. (doi:10.1002/slct.201700261)
- Erande MB, Pawar MS, Late DJ. 2016 Humidity sensing and photo detection behavior of electrochemically exfoliated atomically thin-layered black phosphorus nanosheets. *ACS Appl. Mater. Interfaces* **8**, 11548–11556. (doi:10.1021/acsami.5b10247)
- Late DJ. 2016 Liquid exfoliation of black phosphorus nanosheets and its application as humidity sensor. *Microporous Mesoporous Mater.* **225**, 494–503. (doi:10.1016/j.micromeso.201601031)

32. Li J, Fan HQ, Jia XH. 2010 Multilayered ZnO nanosheets with 3D porous architectures: synthesis and gas sensing application. *J. Phys. Chem. C* **114**, 14 684–14 691. (doi:10.1021/jp100792c)
33. Liu XH, Zhang J, Wang LW, Yang TL, Guo XZ, Wu SH, Wang SR. 2011 3D hierarchically porous ZnO structures and their functionalization by Au nanoparticles for gas sensors. *J. Mater. Chem.* **21**, 349–356. (doi:10.1039/C0JM01800G)
34. Wang XZ, Liu W, Liu JR, Wang FL, Kong J, Qiu S, He CZ, Luan LQ. 2012 Synthesis of nestlike ZnO hierarchically porous structures and analysis of their gas sensing properties. *ACS Appl. Mater. Interfaces* **4**, 817–825. (doi:10.1021/am201476b)
35. Liu JY, Guo Z, Meng FL, Luo T, Li MQ, Liu JH. 2009 Novel porous single-crystalline ZnO nanosheets fabricated by annealing ZnS(en)_{0.5} (en=ethylenediamine) precursor. Application in a gas sensor for indoor air contaminant detection. *Nanotechnology* **20**, 125 501–125 508. (doi:10.1088/0957-4484/20/12/125501)
36. Huang HW, Liu J, He GF, Peng Y, Wu M, Zheng WH, Chen LH, Li Y, Su BL. 2015 Tunable macro-mesoporous ZnO nanostructures for high sensitive ethanol and acetone gas sensors. *RSC Adv.* **5**, 101 910–101 916. (doi:10.1039/C5RA20508E)
37. Chen XS, Liu JY, Jing XY, Wang J, Song DL, Liu LH. 2013 Self-assembly of ZnO nanosheets into flower-like architectures and their gas sensing properties. *Mater. Lett.* **112**, 23–25. (doi:10.1016/j.matlet.201308118)
38. Xu S, Gao J, Wang L, Kan K, Xie Y, Shen PK, Li L, Shi K. 2015 Role of the heterojunctions in In₂O₃-composited SnO₂ nanorods sensor and their remarkable gas-sensing performance for NO_x at room temperature. *Nanoscale* **7**, 14 643–14 651. (doi:10.1039/C5NR03796D)
39. Yang Y, Tian CG, Wang JC, Sun L, Shi KY, Zhou W, Fu HG. 2014 Facile synthesis of novel 3D nanoflower-like Cu₂O/multilayer graphene composites for room temperature NO_x gas sensor application. *Nanoscale* **6**, 7369–7378. (doi:10.1039/c4nr00196f)
40. Yang Y, Sun L, Dong XT, Yu H, Wang TT, Wang J, Yu W, Liu GX. 2016 Fe₃O₄/rGO nanocomposite: synthesis and enhanced NO_x gas-sensing properties at room temperature. *RSC Adv.* **6**, 37 085–37 092. (doi:10.1039/C6RA02306A)
41. Min JH, Liang XY, Wang B, Wang LJ, Zhao Y, Shi WM, Xia YB. 2011 The sensitivity and dynamic response of field ionization gas sensor based on ZnO nanorods. *J. Nanoparticle Res.* **13**, 5171–5176. (doi:10.1007/s11051-011-0500-2)
42. Ahmad MZ, Chang J, Ahmad MS, Wacławik ER, Włodarski W. 2012 Non-aqueous synthesis of hexagonal ZnO nanopyrramids: gas sensing properties. *Sens. Actuat. B Chem.* **177**, 286–294. (doi:10.1016/j.snb.2012.11.013)
43. Sun L *et al.* 2017 Highly active and porous single-crystal In₂O₃ nanosheet for NO_x gas sensor with excellent response at room temperature. *RSC Adv.* **7**, 33 419–33 425. (doi:10.1039/c7ra05446g)
44. Liu Y, Yao S, Yang QY, Sun P, Gao Y, Liang XS, Liu FM, Lu GY. 2015 Highly sensitive and humidity-independent ethanol sensors based on In₂O₃ nanoflower/SnO₂ nanoparticle composites. *RSC Adv.* **5**, 52 252–52 258. (doi:10.1039/C5RA07213A)
45. Li YX, Deng DY, Xing XX, Chen N, Liu X, Xiao XC, Wang YD. 2016 A high performance methanol gas sensor based on palladium-platinum-In₂O₃ composited nanocrystalline SnO₂. *Sens. Actuat. B* **237**, 133–141. (doi:10.1016/j.snb.201606088)
46. Yamazoe N, Fuchigami J, Kishikawa M, Seiyama T. 1979 Interactions of tin oxide surface with O₂, H₂O and H₂. *Surf. Sci.* **86**, 335–344. (doi:10.1016/0039-6028(79)90411-4)
47. Hua ZQ, Wang Y, Wang HQ, Dong L. 2010 NO₂ sensing properties of WO₃ varistor-type gas sensor. *Sens. Actuat. B* **150**, 588–593. (doi:10.1016/j.snb.2010.08.035)
48. Gao F, Qin GH, Li YH, Jiang QP, Luo L, Zhao K, Liu YJ, Zhao HY. 2016 One-pot synthesis of La-doped SnO₂ layered nanoarrays with an enhanced gas-sensing performance toward acetone. *RSC Adv.* **6**, 10 298–10 310. (doi:10.1039/C5RA27270J)
49. Pisarev RV, Pavlov VV, Kalashnikova AM, Moskin AS. 2010 Near-band gap electronic structure of the tetragonal rare-earth cuprates R₂CuO₄ and the bismuth cuprate Bi₂CuO₄. *Phys. Rev. B* **82**, 224502. (doi:10.1103/PhysRevB.82.224502)
50. Yamazoe N, Sakai G, Shimano K. 2003 Oxide semiconductor gas sensors. *Catal. Surv. Asia* **7**, 63–75. (doi:10.1023/A:1023436725457)
51. Morrison SR. 1987 Selectivity in semiconductor gas sensors. *Sens. Actuat.* **12**, 425–440. (doi:10.1016/0250-6874(87)80061-6)
52. Iwamoto M, Yoda Y, Yamazoe N, Seiyama T. 1978 Study of metal oxide catalysts by temperature programmed desorption 4: oxygen adsorption on various metal oxides. *J. Phys. Chem.* **82**, 2564–2570. (doi:10.1002/chin.197909024)
53. Guo Z, Zhao D, Liu Y, Shen D, Zhang J, Li B. 2008 Visible and ultraviolet light alternative photodetector based on ZnO nanowire/n-Si heterojunction. *Appl. Phys. Lett.* **93**, 163501. (doi:10.1063/1.3003877)
54. Bao Q *et al.* 2009 Electrical transport and photovoltaic effects of core-shell CuO/C₆₀ nanowire heterostructure. *Nanotechnology* **20**, 2643–2646. (doi:10.1088/0957-4484/20/6/065203)
55. Hu Z, Xu M, Shen Z, Yu JC. 2015 A nanostructured chromium (III) oxide/tungsten (VI) oxide p-n junction photoanode toward enhanced faradaic efficiency for water oxidation. *J. Mater. Chem. A* **3**, 14 046–14 053. (doi:10.1039/x0xx00000x)
56. Kim HJ, Lee JH. 2014 Highly sensitive, selective gas sensors using p-type oxide semiconductors: overview. *Sens. Actuat. B Chem.* **192**, 607–627. (doi:10.1016/j.snb.2013.11.005)
57. Woo H-S, Na CW, Kim I-D, Lee J-H. 2012 Highly sensitive and selective trimethyl-lamine sensor using one-dimensional ZnO-Cr₂O₃ hetero-nanostructures. *Nanotechnology* **23**, 245501. (doi:10.1088/0957-4484/23/24/245501)
58. Shao F *et al.* 2013 Heterostructured p-CuO (nanoparticle)/n-SnO₂ (nanowire) devices for selective H₂S detection. *Sens. Actuat. B Chem.* **181**, 130–135. (doi:10.1016/j.snb.201301067)
59. Zhang YB, Yin J, Li L, Zhang LX, Bie LJ. 2014 Enhanced ethanol gas-sensing properties of flower-like p-CuO/n-ZnO heterojunction nanorods. *Sens. Actuat. B Chem.* **202**, 500–507. (doi:10.1016/j.snb.201405111)
60. Chen Y, Shen ZR, Jia QQ, Zhao J, Zhao Z, Ji HM. 2015 A CuO-ZnO nanostructured p-n junction sensor for enhanced N-butanol detection. *RSC Adv.* **6**, 2504–2511. (doi:10.1039/C5RA20031H)
61. Jia QQ, Ji HM, Wang DH, Bai X, Sun XH, Jin ZG. 2014 Exposed facets induced enhanced acetone selective sensing property of nanostructured tungsten oxide. *J. Mater. Chem. A* **2**, 13 602–13 611. (doi:10.1039/C4TA01930J)
62. Jia QQ, Ji HM, Zhang Y, Chen YL, Sun XH, Jin ZG. 2014 Rapid and selective detection of acetone using hierarchical ZnO gas sensor for hazardous odor markers application. *J. Hazard. Mater.* **276**, 262–270. (doi:10.1016/j.jhazmat.201405044)
63. Gou X, Wang G, Park J, Liu H, Yang J. 2008 Monodisperse hematite porous nanospheres: synthesis, characterization, and applications for gas sensors. *Nanotechnology* **19**, 125 606–125 606-7. (doi:10.1088/0957-4484/19/12/125606)
64. Jiang S, Gui Z, Chen G, Liang D, Alam J. 2015 Ultrathin nanosheets of organic-modified β-Ni(OH)₂ with excellent thermal stability: fabrication and its reinforcement application in polymers. *ACS Appl. Mater. Interfaces* **7**, 14 603–14 613. (doi:10.1021/acsami.5b04142)
65. Liu JY, Li X, Chen X, Niu H, Han X, Zhang T, Lin HM, Qu FY. 2016 Synthesis of SnO₂/In₂O₃ hetero-nanotubes by coaxial-electrospinning method for enhanced formaldehyde response. *New J. Chem.* **40**, 1756–1764. (doi:10.1039/C5NJ02337H)
66. Zheng ZQ, Zhu LF, Wang B. 2015 In₂O₃ nanotower hydrogen gas sensors based on both Schottky junction and thermoelectronic emission. *Nanoscale Res. Lett.* **10**, 293–306. (doi:10.1186/s11671-015-1002-4)
67. Du HY, Wang J, Sun YH, Yao PJ, Li XG, Yu NS. 2015 Investigation of gas sensing properties of SnO₂/In₂O₃ composite hetero-nanofibers treated by oxygen plasma. *Sens. Actuat. B Chem.* **206**, 753–763. (doi:10.1016/j.snb.201409010)
68. Liu H, Wu SX, Gong SP, Zhao J, Liu JQ, Zhou DX. 2011 Nanocrystalline In₂O₃-SnO₂ thick films for low temperature hydrogen sulfide detection. *Ceram. Int.* **37**, 1889–1894. (doi:10.1016/j.ceramint.201102005)
69. Dong CJ, Liu X, Xiao XC, Chen G, Wang YD, Djerdj I. 2014 Combustion synthesis of porous Pt-functionalized SnO₂ sheets for isopropanol gas detection with a significant enhancement in response. *J. Mater. Chem. A* **2**, 20 089–20 095. (doi:10.1039/C4TA04251D)
70. Trung DD, Hoa ND, Van Tong P, Van Duy N, Dao TD, Chung HV, Nagao T, Van Hieu N. 2014 Effective decoration of Pd nanoparticles on the surface of SnO₂ nanowires for enhancement of CO gas-sensing performance. *J. Hazard. Mater.* **265**, 124–132. (doi:10.1016/j.jhazmat.201311054)
71. Xu S, Gao J, Wang LL, Kan K, Xie Y, Shen PK, Li L, Shi KY. 2015 Role of the heterojunctions in In₂O₃-composite SnO₂ nanorod sensors and their remarkable gas-sensing performance for NO_x at room temperature. *Nanoscale* **7**, 14 643–14 651. (doi:10.1039/c5nr03796d)